xtreme symmetry of the eclipses around inferior conjunction. A full discussion of the various models must be left to a later paper. In summary, however, we believe that the most compelling arguments favour models based on free-free absorption in an ionized medium, despite some serious theoretical difficulties with the production of, and conditions in, the absorbing plasma.

The frequency dependence of the eclipse length first lent credence to free-free absorption mechanisms[3,9,10]. The observed time delays strengthen these models, as radio signals are delayed by propagation through an ionized medium. Using the maximum delay of 500 μs at our observing frequency of 1.67 GHZ gives an electron column density of $\sim 1.0 \times 10^{18}$ cm^{-2} at the closest approach of the line of sight to the pulsar–companion axis. A rough estimate of the electron density comes from dividing this figure by the pulsar–companion separation, 0.85 $R_\odot$, giving $n_e \approx 2 \times 10^7$ cm^{-3}. If we further assume a uniform electron distribution, the plasma temperature required to produce the observed optical depth in a thermal free-free absorption model[11] is ~7,000 K.

A more refined (although still simplified) model was suggested by Rasio *et al.*[9], in which the wind is spherically symmetric about the companion and the electron density drops as $n_e(r) \propto r^{-2}$. Although these are clearly idealizations, the eclipse symmetry does provide some support for these assumptions. (A model incorporating emission of the wind from only the half of the companion nearest the pulsar gives nearly the same results.)

The model incorporates the inclination of the orbit to the line of sight, which is unknown, except that it must be large enough for the line of sight not to intersect the companion, yet small enough to allow the eclipse modulation to be seen. We assume an impact parameter at inferior conjunction of twice the Roche lobe radius, $2r_R \approx 0.3R_\odot$, noting that our conclusions will be rather insensitive to this assumption.

In this model, the free electron density is again calculated from the observed delays during eclipse: $n_e(r) \approx 6 \times 10^7$ cm^{-3} $(r/r_R)^{-2}$. In the free-free absorption model, the electron temperature can be calculated in two extreme cases[9]: an isothermal wind, $T(r) = T_R$, and an adiabatically cooled wind, $T(r) = T_R(r/r_R)^{-4/3}$. From the observed optical depth at inferior conjunction, the required electron temperature is $T \approx 3{,}600$ K for the isothermal case and $T(r) \approx 15{,}000(r/r_R)^{-4/3}$ K for the adiabatic case. The similarity of these results to our previous rough calculation suggests that similar general results can be expected from less idealized assumptions.

The low temperatures predicted are the primary difficulty with free-free models. For thermal ablation to occur, the companion's surface must be extremely hot. For a $0.1M_\odot$, $0.1R_\odot$ companion, the 'escape temperature' for hydrogen is roughly 6×10^6 K, and it is far from clear how to cool the material rapidly to the observed temperatures. A complete free-free model must therefore include either an efficient cooling mechanism, or a nonthermal source for the companion wind, such as Roche lobe overflow.

Assuming this objection can be overcome, we can use the observed electron density to estimate the rate of mass loss from the companion, and hence how long it will last. If the wind has velocity v and ionization fraction ξ (which is frozen in after ablation, as the wind is far from ionization–recombination equilibrium[10]), then the evaporation timescale is

$$\left(\frac{m}{\dot{m}}\right) = \left(\frac{m\xi}{4\pi r_R^2 \rho_R v}\right) \approx 700\xi \left(\frac{v}{v_{orb}}\right)^{-1} \text{Gyr}$$

where $v_{orb} = 6 \times 10^7$ cm s^{-1} is the companion's orbital velocity. For ionization fractions greater than a few per cent and any reasonable values of v, this time is greater than the Hubble time, indicating that ablation alone may be insufficient to leave PSR1744−24A as an isolated millisecond pulsar. □

Received 20 May; accepted 9 September 1991.

1. Lyne, A. G. *et al. Nature* **347,** 650–652 (1990).
2. Nice, D. J., Thorsett, S. E., Taylor, J. H. & Fruchter, A. S. *Astrophys. J.* **361,** L61–L63 (1990).
3. Rasio, F. A., Shapiro, S. L. & Teukolsky, S. A. *Astr. Astrophys.* **241,** L25–L28, (1991).
4. Ruderman, M., Shaham, J. & Tavani, M. *Astrophys. J.* **336,** 507–518 (1989).
5. Ruderman, M., Shaham, J., Tavani, M. & Eichler, D. *Astrophys. J.* **343,** 292–312 (1989).
6. Fruchter, A. S. *et al. Astrophys. J.* **351,** 642–650 (1990).
7. Michel, F. C. *Nature* **337,** 236–238 (1989).
8. Eichler, D. *Astrophys. J.* **370,** L27–L30 (1991).
9. Rasio, F. A., Shapiro, S. L. & Teukolsky, S. A. *Astrophys. J.* **342,** 934–939 (1989).
10. Wasserman, I. & Cordes, J. M. *Astrophys. J.* **333,** L91–L94 (1988).
11. Rybicki, G. B. & Lightman, A. P. *Radiative Processes in Astrophysics* (Wiley, New York, 1979).

ACKNOWLEDGEMENTS. We thank M. McKinnon for observational assistance at the VLA and J. Taylor for helpful comments on the manuscript. The NRAO is operated by Associated Universities, Inc., under contract from the NSF. This research was supported by the NSF and the U.S. Department of Education.

Observation of quantum supershells in clusters of sodium atoms

J. Pedersen*, S. Bjørnholm*, J. Borggreen*, K. Hansen*, T. P. Martin† & H. D. Rasmussen*

* The Niels Bohr Institute, University of Copenhagen, Blegdamsvej 17, DK-2100 Copenhagen Ø, Denmark
† Max-PLanck-Institut für Festkörperforschung, Heisenbergstrasse 1, D-7000 Stuttgart 80, Germany

ATOMIC clusters of sodium and other simple metals are known to exhibit a shell structure, giving rise to enhanced stability at certain 'magic numbers' of constituent atoms[1–3]. Balian and Bloch have shown[4] that such shells are the likely result of particularly stable electronic structures: electrons in a spherical cavity (approximating the potential in the clusters) follow semiclassical triangular or square orbits, leading to a shell structure similar to that in atoms[5], and stable configurations occur at magic numbers proportional to the cube root of the number of electrons. Balian and Bloch[4] also predicted that the existence of both triangular and square orbits, with slightly different periodicities of their magic numbers, should lead to a 'quantum beating' effect that imposes a low-frequency envelope on the periodic variation in cluster stability with increasing size, in effect creating an additional 'supershell' structure. Here we report the observation of this supershell effect in sodium clusters with up to 3,000 constituent atoms.

The semiclassical theory of Balian and Bloch[4] was extended and applied to idealized spherical sodium droplets with somewhat diffuse potential walls[6]. A quantum beat was found in the shell structure, with a pronounced minimum being predicted around size $N = 1{,}000$. The semiclassical results were compared to and found to agree fairly closely with the eigenvalue spectrum obtained by solving the stationary Schrödinger equation for independent electrons in the same potential. In hydrogen there is a one-to-one relation between a classical orbit and the corresponding quantum eigenstate. Both pictures predict the well-known shell structure in hydrogen. With potentials like those of a spherical metal cluster, the one-to-one correspondence between individual classical and quantum 'orbits' is lost. Nevertheless, the bunching of quantum levels into shells can still be understood[4,6] in terms of the system of closed orbits (polygons with more or less rounded corners) available to a classical particle moving in the same potential. From this description it becomes possible to see that the quantum beat mode results from an interference between classical triangular and square orbits, because these emerge as the dominant and equally important contributors to the quantum shell structure[4,6].

Experiments have shown that the spherical mean field assumption used in the shell structure calculations is valid for sodium clusters extending in size beyond 600 (ref. 7), possibly even to $N \leq 1{,}400$ (ref. 8). A recent laser warming experiment[9]

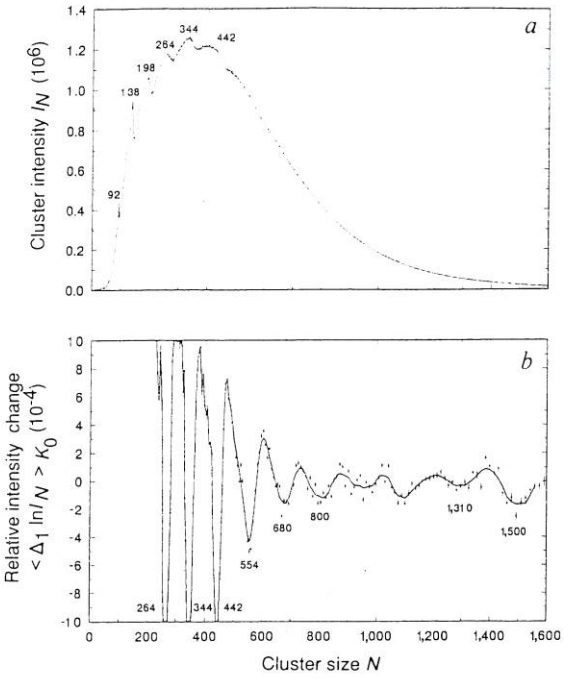

FIG. 1 Mass spectrum and its logarithmic derivative. *a*, Example of an abundance distribution for sodium clusters produced by adiabatic expansion and measured after 1 m free flight by time-of-flight mass spectrometry. *b*, Logarithmic derivative $\langle \Delta_1 \ln I_N \rangle_{K_0}$ of the results in top panel according to eq. (2).

provides additional evidence for the existence of quantum shells up to $N \leq 2{,}500$ in sodium.

Our experiment is based on measurements of the size distribution of metal droplets produced by expansion of metal vapour through a fine nozzle. Sodium vapour is generated in a stainless steel vessel held at 700–800 °C, and the expansion is assisted by pressurizing the vessel with a large surplus of argon or xenon gas. The mixture is expanded into a 3-m-long, differentially pumped flight tube, resulting in a narrow beam of free-flying metal clusters with velocities close to the initial thermal speed of the argon or xenon atoms[7]. In the expansion and clustering process, lasting about 100 ns, the noble gas medium cools to a few tens of kelvin[2]. In the sodium clusters, on the other hand, there will be a competition between heating, due to condensation, and cooling, due to collisions. We believe that the resulting internal temperature in the freshly formed clusters is ~100–200 °C below the oven temperature. In the ensuing free flight (for ~1 ms) the droplets will therefore lose sodium atoms by stepwise evaporation, cooling to ~100–200 °C. This evaporation process is sensitive to shell-like variations in the atomic separation energies; and these variations are thought to be responsible for the step-like modifications of the experimentally observed size distributions[7,10], although the pre-evaporation size distributions are presumably completely smooth.

The size distribution is sampled 1 m downstream by time-of-flight mass spectrometry[7]. Ultraviolet photons with energies close to the ionization threshold and an energy spread of 1 eV (compared with a total Fermi energy in sodium of 3.24 eV) are used to produce a representative sample, in the form of ions, from the otherwise neutral size distribution. Figure 1*a* shows an example of an abundance distribution I_N against N obtained in this way. For sizes up to $N = 300$, the bell-shaped abundance distribution is clearly scarred with saw-tooth or *s*-shaped irregularities at certain 'magic' sizes. As the interest focuses on these, it is convenient to display the experimental result in terms of relative intensity changes:

$$\Delta_1 \ln I_N = \ln (I_{N+1}/I_N) \approx 2\frac{(I_{N+1} - I_N)}{(I_{N+1} + I_N)} \qquad (1)$$

This makes the magic numbers, N_0, stand out very clearly as dips[7]. As one sees from Fig. 1*a*, the steps signalling shell closures tend to be obscured by noise due to finite counting statistics for the higher N-values. In this situation we have found it useful to generalize equation (1). This is achieved by calculating a weighted logarithmic derivative for properly spaced mass points N,

$$\langle \Delta_1 \ln I_N \rangle_{K_0} = \frac{\sum_{K=2K_0/3}^{K_0} 2(I_{N+1+K} - I_{N-K})(2K+1)/(I_{N+1+K} + I_{N-K})}{\sum_{K=2K_0/3}^{K_0} (2K+1)^2} \qquad (2)$$

choosing values of $K_0 = 0.03N$. The derivative is thus sampled over intervals of $2K_0+1$, which is ±3% of the actual size. In this way we can scale up the measured derivatives in order to display small irregularities in the intensity pattern. Figure 1*b*

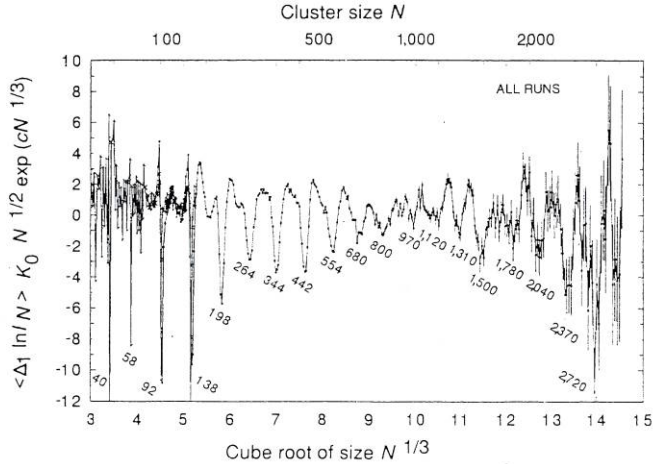

FIG. 2 The quantum beat. Relative changes $\langle \Delta_1 \ln I_N \rangle_{K_0}$ in experimental cluster abundance I_N, corrected for the effect of temperature and size. The model considerations behind the corrections are described in refs 11–13. Measurements from ref. 7 are also shown (crosses). The logarithmic amplitudes $\Delta_1 \ln I_N$ are scaled by an extra factor of 0.2 to account for the superior mass resolution and the use of equation (1) instead of equation (2) for these data.

shows the result. There is a strong decrease in the amplitudes of the shell dips with little or no sign of a beat mode.

There are two reasons for this decrease. First, shell structure is due to periodic variations in an otherwise uniform single-particle electron level density. In a medium of constant density with constant Fermi energy, or, equivalently, constant width of the conduction band, the spacing $\hbar\omega_{\text{shell}}$ between consecutive modulations will decrease as $1/n$ where n is the number of occupied shells. This will cause a decrease proportional to $N_0^{-1/3}$ in the expected dips[6,7], as n is proportional to $N_0^{1/3}$. If furthermore, the amplitudes of the shell modulations decrease as $N_0^{-1/6}$, the overall decrease will vary[11] as $N_0^{-1/2}$, even at zero absolute temperature. Second, more importantly, temperature[10,12,13] tends to wash out the observable shell structure. The effect increases exponentially[11] in the effective temperature parameter τ,

$$\tau = k_B T \frac{2\pi^2}{\hbar\omega_{\text{shell}}} \tag{3}$$

with

$$\hbar\omega_{\text{shell}} \approx 2\varepsilon_F/n \propto N^{-1/3} \tag{4}$$

Here, k_B is Boltzmann's constant, T is the real temperature at the time of sampling the abundance distributions, estimated[14] to be 400–500 K, and $\varepsilon_F = 3.24$ eV is the Fermi energy.

To compensate for these effects, we have scaled the experimental logarithmic derivatives, $\langle \Delta_1 \ln I_N \rangle_{K_0}$ (see Fig. 1*b*) by the factor $N^{1/2} \exp(cN^{1/3})$, setting $c = 0.65$. The results are presented in Fig. 2. They are plotted as a function of the linear dimensions of the clusters, $\sim N^{1/3}$, and comprise all results from our series of experiments, supplemented with some previous results[7] from the lower size range. The shell dips are equidistant, as expected from theory[4]. In addition, the amplitudes of the dips vary systematically. As the scaling function increases monotonously, it cannot by itself introduce the large-scale modulations seen in Fig. 2. These have the character of a beat mode with a minimum near $N = 1{,}000$, as predicted by semiclassical theory[4,6].

As a further verification of this quantum beat, Fig. 3 presents a plot of the cube root of the magic numbers, $N_0^{1/3}$, against the running index, n, which represents the period (or shell) number. The simplest representation of a beat mode is the sum of two cosine functions of n with slightly different wave numbers $k_\triangle$ and $k_\square$, and $k_\triangle + k_\square = 4\pi$:

$$\cos(k_\triangle n) + \cos(k_\square n) = 2\cos\left(\frac{k_\triangle + k_\square}{2} n\right) \times \cos\left(\frac{k_\triangle - k_\square}{2} n\right) \tag{5}$$

The minima of this function will be equidistant, sharing a phase shift of $\frac{1}{2}n$ each time the envelope factor changes sign, that is, with each new superperiod. As seen in Fig. 3, the experimental data show exactly these features. The plot is linear in $N_0^{1/3}$ and there is a phase shift of $1/2n$, which occurs just where the intensities (Fig. 2) pass through a minimum. A plot of the theoretically predicted shell closures[6] has the same two features. Note that the results of Fig. 3 can be obtained directly from the experimental data, before any correction for the effect of size and temperature is introduced).

The length of the shell periods, implied by the slope factor 0.61 ± 0.01) from Fig. 3, also supports an interpretation in terms of classical triangular and square orbits. In connection with an earlier study, extending only to $N = 600$, we have shown[7] that electrons moving classically in triangular and square orbits of total length L will have integer action values, $pL = nh$ for sizes N_s spaced at intervals $\Delta N_s^{1/3} = 0.61$, if they have an average momentum p equal to the Fermi momentum in sodium metal (or a wavelength equal to the Fermi wavelength). For other

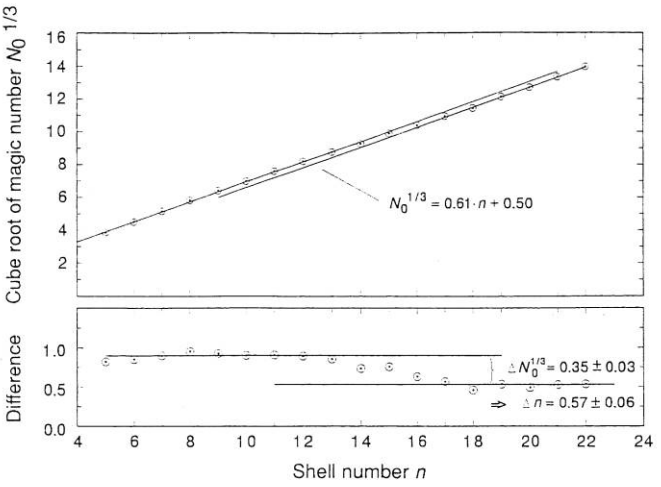

FIG. 3 The phase shift. *a*, Cube root of the magic numbers from Fig. 2, signifying shell closures, plotted against shell number n. For higher shell numbers the points fall on two straight lines, phase-shifted by $\frac{1}{2}n$. This is shown more clearly in *b*, where a straight line has been subtracted from the data above.

sizes, the average momentum and energy of the least bound particles will have to be slightly larger or smaller to fulfill Bohr's quantization condition. This is one way of explaining the shell oscillations. The beat mode comes about because the lengths L of triangular and square orbits differ slightly.

In summary, we have shown that the conduction electrons in droplets of sodium metal form a quantum system with periodic shell structure in analogy to the periodic system of the atomic electrons. The measurements have been extended to drops containing 3,000 conduction electrons. Altogether, 22 shell periods have been identified and found to form a beat pattern in the amplitude of the shell effect, where ~10 adjacent shells are grouped together into a supershell. These features agree with the semiclassical theory of Balian and Bloch[4], describing the quantal shell structure in terms of closed classical orbits. Sodium clusters therefore form a suitable model system for the study of shells with large quantum numbers, where the correspondence between ordered classical motion and quantum shell structure becomes apparent.

The experiments are performed with clusters having finite temperatures, whereas the theories apply to zero temperature. As a result, the observable effects are hundreds of times smaller than the zero-temperature predictions. The survival of measurable effects indicating systematic interference between distinctly different triangular and square orbits despite overwhelming thermal noise is one of the surprising results to emerge from our work. □

Received 9 May; accepted 15 August 1991.

1. Knight, W. D. *et al. Phys. Rev. Lett.* **52,** 2141–2144 (1984).
2. de Heer, W. A., Knight, W. D., Chou, M. Y. & Cohen, M. L. *Solid State Phys.* **40,** 93–181 (1987).
3. Katakuse, I. *et al. Int. J. Mass Spectrom. Ion Proc.* **67,** 229–236 (1985).
4. Balian, R. & Bloch, C. *Ann. Phys.* **69,** 76–160 (1972).
5. Bjørnholm, S. *Contemp. Phys.* **31,** 309–324 (1990).
6. Nishioka, H., Hansen, K. & Mottelson, B. R. *Phys. Rev.* B**42,** 9377–9386 (1990).
7. Bjørnholm, S. *et al. Phys. Rev. Lett.* **65,** 1627–1630 (1990).
8. Martin, T. P., Bergmann, T., Göhlich, H. & Lange, T. *Chem. Phys. Lett.* **172,** 209–213 (1990).
9. Martin, T. P. *et al. Chem. Phys. Lett.* (in the press).
10. Bjørnholm, S. *et al. Z. Phys.* D**19,** 47–50 (1991).
11. Bohr, A. & Mottelson, B. R. *Nuclear Structure* Vol. II, 608 (Benjamin, London, 1975).
12. Brack, M., Genzken, O. & Hansen, K. *Z. Phys.* D**21,** 65–81 (1991).
13. Brack, M., Genzken, O. & Hansen, K. *Z. Phys.* D**19,** 51–53 (1991).
14. Brechignac, C., Cahuzac, Ph., Leygnier, J. & Weiner, J. *J. Chem. Phys.* **90,** 1492–1498 (1989).

ACKNOWLEDGEMENTS. We thank O. Echt, W. D. Knight and B. R. Mottelson for advice and encouragement.